A Microstructural Study of Local Melting of Gray Cast Iron with a Stationary Plasma Arc

Control of heat input and filler metal composition significantly influences the welding of gray cast iron with the plasma arc process

BY T. ISHIDA

ABSTRACT. Microstructural changes in the fusion region, deposited filler metal, fusion boundary region and heat-affected zone (HAZ) of flake graphite cast iron locally melted by plasma arc with and without the addition of filler metal were investigated. A cylindrical base metal specimen of 35 mm (1.38 in.) in diameter and 25 mm (0.98 in.) in height was locally melted at fixed time intervals with a static plasma torch using argon plasma gas and Ar+10%H_2 shielding gas. When a filler metal was used, it was inserted into the plasma arc and deposited on the base metal. The cooling rate in the fusion region was recorded. Evaluation of fusion boundary area included metallurgical analysis, microhardness test and electron probe microanalysis.

When filler metal is not used, the structure in the fusion region is ledeburite eutectic due to a high cooling rate. In the center of the fusion region, hypoeutectic white cast iron seems to be present and in the vicinity of the fusion boundary of this region where fine ledeburite eutectic appears. In the fusion boundary region where super cooled phenomenon can occur, minute martensite precipitates along the fusion line when the heat input is low and secondary graphite precipitates when the heat input is high. The HAZ is composed of white martensitic, dark martensitic and martensitic-fine pearlitic layers when the heat input is high. Carbon solid solution from flake graphite in the matrix occurs mostly in the HAZ; however, no evidence of melting due to a partial lowering of the melting point of the matrix immediately adjacent to the flake graphite is apparent.

When filler metal is used, the structure of the deposit filler metal is that of a Ni austenitic matrix which precipitates tiny graphite nodules or slim graphite for Ni and Ni-Fe filler metals and a pearlitic matrix for Fe filler metal. In the fusion boundary region, Ni-martensite, eutectic or slim graphite and minute Ni-martensite are precipitated with Ni-based filler metals. A columnar structure of ferrite and pearlite is obtained with Fe-based filler metal. The structure in the HAZ varies with the difference in the melting point of the filler metal. The HAZ is composed of thin iron carbide, martensitic, martensitic-fine pearlitic and fine-laminated pearlite layers for Ni filler metal, of iron carbide and fine-laminated pearlite layers for Ni-Fe filler metal and of thick iron carbide, eutectic graphite-crystallized and fine-laminated pearlite layers for Fe filler metal. The carbide layer in the HAZ is thicker for Fe filler metal than for Ni or Ni-Fe filler metals because of the difference in the freezing points of the filler metals. The hardness of the iron carbide and Ni-martensitic layers is very high where melting occurred with the exception of the carbide layer of the Fe filler metal. It is noted that from the Ni concentration gradient in the carbide layer, the diffusion of Ni from the deposit metal into the HAZ can occur at least until the base metal is fused.

Introduction

It has recently been shown that the availability of high powered and continuous energy sources such as laser (Ref. 1), electron beam (Refs. 1, 2) and plasma arc (Ref. 4) lead to the development of new materials processing techniques. One such process is a rapid melting and subsequent solidification of metallic substrates. In the present investigation, a high powered plasma arc is used for rapid surface melting and solidification of gray cast iron to determine the feasibility of employing this process in the welding of gray cast iron. It is anticipated that the utilization of the plasma arc process to weld or repair-weld large gray iron castings would be justified because of the improvement in the structural integrity of the cast iron that such a process affords. There is very little literature (Refs. 5, 6) or basic research pertaining to the welding of gray cast iron. One such study, though, by Devletian (Refs. 7, 8) on the arc welding of gray cast iron using gray iron electrodes, has demonstrated that the weldability of gray iron is significantly affected by the cooling rate and carbon equivalent of the weld metal and that gray iron weld metal containing optimum aluminum addition exhibits substantial graphitization and reduced hardness. In the gray cast iron weldment, the microstructure is characterized by the formation of iron carbide and martensite in the heat affected zone (HAZ). This iron carbide layer forms in the molten iron region of the fused and diluted base metal adjacent to the fusion region due to a fast cooling rate. The formation of iron car-

T. ISHIDA is with the Department of Metallurgical Chemistry at The Research Institute for Iron, Steel and Other Metals, Tohoku University, Sendai, Japan.

Table 1—Chemical Composition of FGI, wt-%

	C	Si	Mn	P	S	C.E.[a]	Matrix
Base metal	3.49	2.24	0.59	0.016	0.015	4.2	pearlite

a) Carbon Equivalent = %C + 0.3(%Si + %P)

bide may be avoided by adequate alteration of the chemical composition in the molten iron region. This alteration results from the diffusion of filler metal into the molten iron region. It is possible to make filler metal diffuse into the molten iron region by the use of the plasma arc process. The formation of martensite in the HAZ occurs in the area immediately adjacent to this carbide region. Large amounts of carbon can be dissolved in the austenite during the heat cycle by solution of carbon from flake graphite, and on rapid cooling, high carbon martensite will form. This martensite formation is partially eliminated by a high preheat to lower the cooling rate; however, the use of the plasma arc process with a suitable filler metal will also eliminate the martensite.

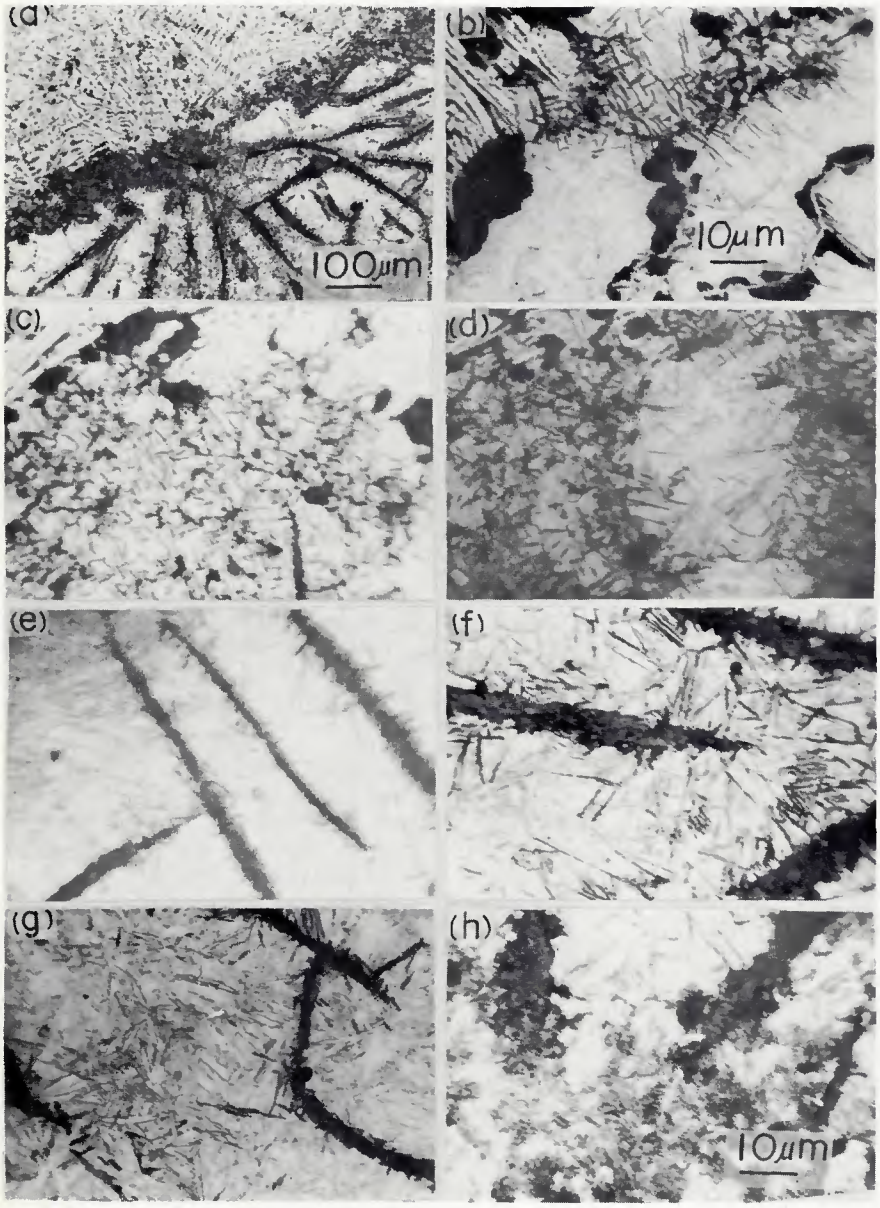

Fig. 1—Microstructures of fusion boundary and HAZ of FGI locally melted by plasma arc for 15 s (Nital etch). A—Fusion boundary area; B—Minute martensites along the fusion line; C, D—Minute martensites surrounding slender flake graphite in the neighboring carbide and eutectic; E—White martensite in the neighborhood of the fusion line; F—Black-etched martensite bordering flake graphite; G—Dark, fine martensite far from the fusion line; H—Martensite-fine pearlite structure

The purpose of this study is to elucidate the microstructural changes of flake graphite, cast iron (FGI) in discrete regions produced by local melting with a stationary plasma arc. Furthermore, it is to establish a sound mechanism for origin of the fusion boundary when Ni, Ni-Fe and Fe filler metals are deposited. In so doing, a better understanding of the basic plasma arc welding of gray cast iron is reached. Specifically, this paper discusses the interfacial microstructures of the fusion boundary and the HAZ, microhardness and components across the fusion boundary.

Experimental Procedures

The chemical composition of the flake graphite cast iron (FGI) used in this study is indicated in Table 1. FGI was produced from reduction melting (Ref. 9) in an electric furnace into which steel scrap was added to pig iron. The molten iron was cast into a sand mold 40 mm (1.58 in.) in diameter. The predominant microstructure in these castings is a pearlitic matrix with flake graphite. The castings were cut into specimen cylinders 35 mm (1.38 in.) in diameter and 25 mm (0.99 in.) in length. The filler metals were provided from 10 mm (0.39 in.) diameter metal mold castings of deoxidized and degassed vacuum-melted electrolytic nickel and iron. The filler metal used in the experiment was forged and rolled wire rod with a 4 mm (0.16 in.) diameter and a 200 mm (7.9 in.) length. Commercial welding rods CIA-1 (AWS ENi-CI) and CIA-2 (AWS ENiFe-CI) were also used.

The heat source for the local melting was a transferred plasma arc welding machine (Hitachi-300A). The base metal cylinder was placed on a copper plate 15 × 100 × 100 mm (0.59 × 3.94 × 3.94 in.) situated on an iron table and was melted locally under the static plasma torch at fixed time intervals. When filler metal was used, it was inserted into the plasma arc and deposited onto the base metal. Arc time measurement commenced simultaneously with the transfer of the main arc. The actual arc time of the main arc was from 10 to 40 sec. The welding current was 130A. The plasma gas was argon with a flow rate of 2.8 dm^3min^{-1}, and the shielding gas was Ar+10%H_2, with a flow rate of 13.0 dm^3min^{-1}. The electrode used was tungsten with a 6 mm (0.24 in.) diameter. The nozzle diameter was 3 mm (0.12 in.), and the distance from nozzle to base metal was 8–10 mm (0.32–0.39 in.). The shielding gas continued for a fixed time after the disappearance of the arc. After local

Table 2—Averaged Thickness and Hardness of Each Region of Three Layers in the HAZ Heated by Plasma Arc for 15 s

HAZ	Thickness of each region in the bead (mm) Center	Near to edge	Vickers microhardness, H_v
White martensite layer	0.186	0.295	677
Dark martensite layer	0.310	1.183	674
Martensite-fine pearlite layer	0.319	0.699	352

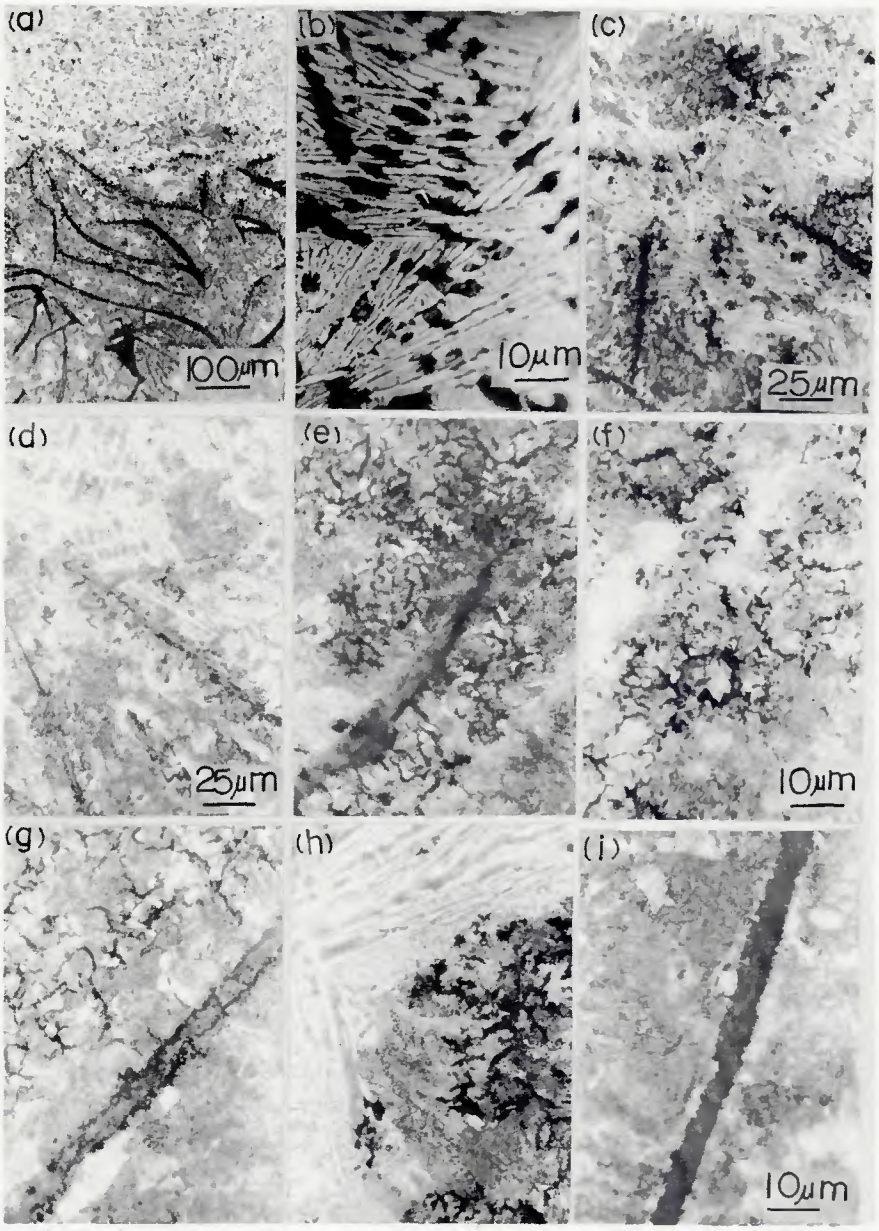

Fig. 2—Microstructures of fusion boundary and HAZ of FGI locally melted by plasma arc for 25 s (Nital etch). A—Fusion boundary area; B—Ledeburite in fusion region; C—Fusion line region between ledeburite and pearlite; D—Slender graphites retained as nonfusion graphite in the ledeburitic region; E—Tiny graphites precipitated around reduced flake graphite; F—Tiny graphites precipitated during solidification from liquid phase; G—Tiny graphites precipitated in the neighborhood of flake graphite; H—Tiny graphites and pearlitic matrix in contact with ledeburite; I—Flake graphite with finely laminated pearlite matrix at HAZ

melting by the plasma arc was carried out with or without filler metal, and the specimens were cooled to room temperature on the iron table, they were cross-sectioned, polished and then etched in 5% nital. Those with filler metal deposit were analyzed across the deposit fusion boundary region with the help of electron probe microanalysis (EPMA), and a Vickers microhardness was taken.

To obtain the cooling curves of the melted region, the temperature was measured by plunging a 0.5 mm (0.02 in.) diameter Pt/Pt-13 %Rh thermocouple directly into the molten pool after the arc had just disappeared. Cooling curves were recorded on a continuous chart recorder and an average cooling rate for each specimen was taken at the temperature drop from 1000°C to 900°C (1832°F–1652°F). The value of the cooling rate obtained was 23°C/s (73.4°F/s) for an arc time of 15 seconds, 20°C/s (68°F/s) for an arc time of 20 sec, 13.5°C/s (56.3°F/s) for an arc time of 30 sec and 12.5°C/s (54.5°F/s) for an arc time of 35 sec.

Results

Without the Use of Filler Metal

There is a great difference in the fusion boundary area structure resulting from the duration of the plasma arc (i.e., the variation of heat input). This phenomenon is considered to depend upon the cooling rate. The microstructural changes in the fusion region, the fusion boundary region and the HAZ as effected by heat input are described in the following:

Low Heat Input. Figure 1 shows solidified microstructures in the fusion boundary area of FGI when locally melted by a plasma arc of 15 second duration. As shown in Fig. 1A, the fusion region becomes white iron and the HAZ is martensitic. Since the arc time is very short and the heat input is low, the region of the fusion is shallow and narrow, and the cooling rate is very high. The cooling rate in this fusion region is 23.0°C/s (73.4°F/s). In this case, a rapid cooling structure appears in the fusion region and the HAZ. This fusion boundary area contains the following three regions of interest:

1. Fusion Region—Cast iron directly under the plasma arc is completely melted and immediately after the arc disappears the liquid rapidly solidifies as white iron containing massive iron carbide and pearlite without effective nuclei for graphite. Accordingly, in this region the structure is ledeburitic eutectic in the absence of graphite.

2. Fusion Line—The demarcation between white iron and a martensitic matrix is the fusion line. As shown in Fig. 1B, minute martensites appear along the

fusion line, and the matrix adjacent to the fusion line is a white martensitic structure surrounded with fine pearlite. As shown in Figs. 1C and D, minute martensites surround the slender flake graphite adjoining the white iron. The vicinity of the fusion line is subjected to a rapid heating from the molten region and a rapid cooling from the base metal.

3. HAZ—This region is primarily a martensitic matrix with flake graphite. The martensite becomes fine and fine pearlite begins to appear away from the fusion line. This area, which ranges from the fusion line to the base metal, is composed of four major sections:

- White martensite layer—The lightly etched martensite adjacent to the fusion line as shown in Fig. 1E, is white martensite, which is considered to be tetragonal martensite. Martensite immediately adjacent to the flake graphite is black-etched and needle-like—Fig. 1F. As indicated in Fig. 1C, flake graphite in the vicinity of the fusion line is slenderized by dissolution and diffusion of carbon into the austenitic matrix during the heat cycle. In this region, there is a significant migration of carbon from flake graphite into austenite, and with rapid cooling high carbon austenite transforms into coarse martensite and the matrix immediately adjacent to flake graphite may be in a carbon-supersaturated state.
- Dark martensite layer—At a distance from the fusion line, dark-etched and fine martensite is present, as shown in Fig. 1G. This martensite is similar to that found with short-time tempering, and is thought of as cubic martensite. Tetragonal martensite transforms to cubic martensite precipitating ϵ-carbide. Therefore, the martensite is visible primarily as black-etching.
- Martensite-fine pearlite layer—With more distance from the fusion line, much fine pearlite appears in the neighborhood of the flake graphite. As shown in Fig. 1H, a structure combining fine martensite and pearlite is observed. In this region, migration of carbon into the matrix can occur also.
- Fine-laminated pearlite structure—Pearlite in the matrix becomes fine-laminated near the base metal. In this region, carbon migration into the matrix has scarcely occurred.

Averaged layer thickness and hardness of each region of the HAZ is presented in Table 2. The layer thickness is larger at the edge of the bead than in the center.

High Heat Input. Figure 2 shows solidified microstructures in the fusion boundary area of FGI which was locally melted by plasma arc for 25 seconds. Cooling rate in this fusion region is 17.0°C/s (62.6°F/s). As heat input from plasma arc increases as a result of long arc time, the melted zone is enlarged and temperature of the molten metal is increased. Therefore, the cooling rate in the fusion boundary and HAZ is low and a slowly cooled structure appears in each region. As shown in Fig. 2A, the fusion region becomes white iron and the HAZ is fine-laminated pearlite. Microstructural changes of each region are described in the following:

1. Fusion region—As shown in Fig. 2B this region is white iron with massive iron carbide and eutectic. For an arc time longer than 25 seconds, constituent variation may occur in this region. In the center of the fusion region, hypoeutectic white cast iron is thought to solidify, but in the vicinity of the fusion boundary, fine ledeburite is present.

2. Fusion line—Demarcation between the ledeburitic structure and pearlitic one is the fusion line—Fig. 2C. As shown in Fig. 2D, flake graphite existing in the ledeburitic structure remains slender as undissolved graphite. As shown in Fig. 2E, in the area surrounding the slenderized graphite, a great amount of small graphite appears in the pearlitic matrix towards the ledeburite eutectic. As indicated in Figs. 2F and G, the graphite melted completely and small graphites were crystallized during solidification. Whereas, Fig. 2H shows that the matrix of pearlite containing these graphites adjoins the ledeburitic structure. These graphites are less in the center of the bead, but increase towards the edges. The form of graphite flakes observed in the fusion line is similar to the interdendritic ASTM types D and E (Ref. 10). However, the size is smaller than that of D and E types.

3. HAZ—Greater heat from the melted zone obviates martensite formation in the HAZ and a fine-laminated pearlite structure is obtained with a high preheat as described in the following:

- Fine-laminated pearlite layer—The matrix is fine-laminated with pearlite as shown in Fig. 2I and this layer becomes relatively thicker.
- Laminated-pearlite-ferrite mixed layer—At a distance from the fusion line, ferrite appears in a position far from the graphite flake. This ferrite exists only at positions where the diffusion of carbon is very limited.
- Fine-laminated pearlite layer—Pearlite becomes fine-laminated and ferrite also exists.

Table 3—Averaged Thickness and Hardness of Two Layers in the HAZ Heated by Plasma Arc for 25 s

HAZ	Thickness of each layer in the bead (mm) Center	Near to edge	Vickers microhardness, H_V
Pearlite layer	1.6	1.8-3.55	431
Pearlite-Ferrite layer	1.4	1.9	369

The averaged thickness and microhardness of each layer in the HAZ for high heat input is given in Table 3. Each layer is thicker in the circumference than in the center, especially the fine-laminated pearlite layer.

With the Use of Filler Metal

Ni Filler Metal. Figure 3 shows solidified microstructures of deposit fusion boundary area of FGI when Ni filler metal is introduced into the plasma arc. Microstructural changes of each region are described in the following:

1. Deposit metal (DM)—In this region, Ni-Fe-C alloy is formed constituently by the dilution of base metal (Ref. 11). Tiny spheroidal graphite is crystallized within this region, as indicated in Fig. 3A. It is particularly numerous in the vicinity of the fusion boundary. At locations in close proximity to the fusion boundary, graphite flakes are observed, as shown in Fig. 3B.

2. Fusion boundary region—In the center and at the edges of the bead, Ni-martensite (Refs. 12, 13) adjoins ledeburitic structure, as shown in Fig. 3C. In an area of the center, as shown in Fig. 3D, small and tiny flake graphite-crystallized Ni alloy adjoins eutectic graphite and minute Ni-martensite. The flake graphite remains slender as undissolved graphite, and is joined to the base metal without ledeburite eutectic. Thus, in this fusion boundary region Ni-martensite (Ref. 14), undercooled graphite, minute Ni-martensite and ledeburite eutectic are formed by a rapid cooling during solidification.

3. HAZ—In the iron carbide layer, a relatively thin layer of ledeburitic structure appears in the center and at the edges of the bead, as shown in Fig. 3E. In the area from the center to the edges, the ledeburitic structure disappears. The portion where iron carbide appears is a partially melted region of the base metal due to the heat from the deposit metal side.

In the martensitic layer, the martensite near the fusion line side has a large needle-like structure. Away from the fusion line, the martensite becomes fine and fine pearlite also exists. Martensite adjoining the ledeburite eutectic precipitates with fine pearlite around the bound-

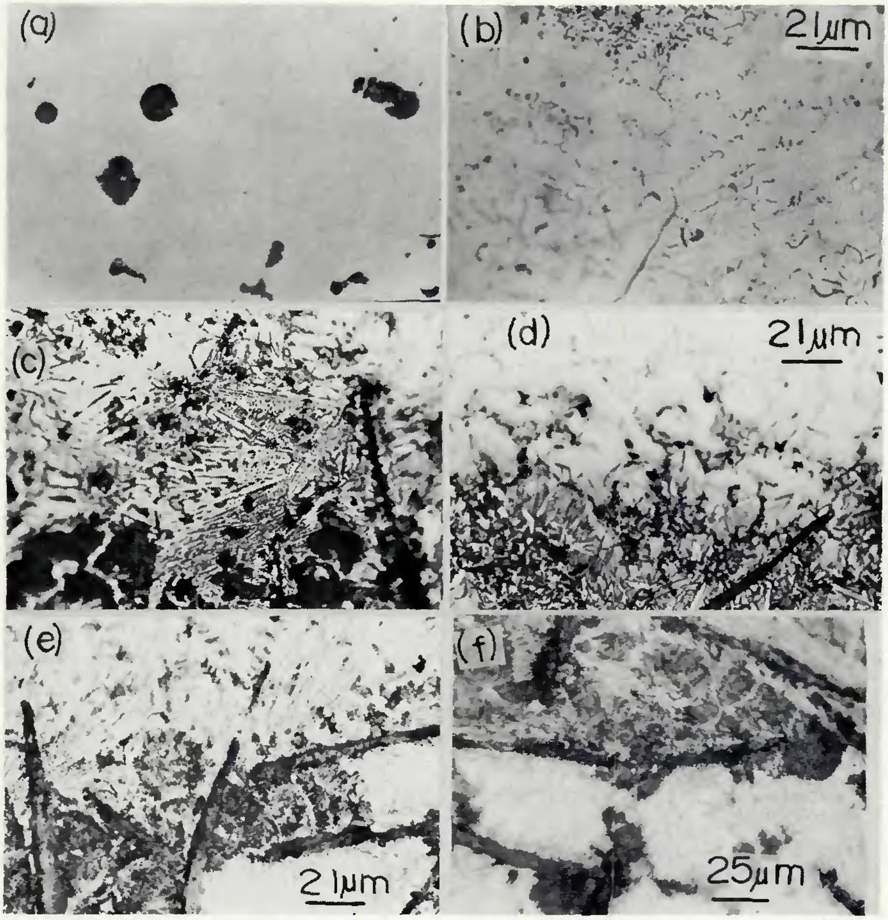

Fig. 3 — Microstructures of deposited fusion boundary area with Ni filler metal added by plasma arc (Nital etch). A — Tiny graphite nodules in Ni austenitic matrix of deposited metal; B — Tiny graphite flakes adjacent to fusion boundary in deposited metal; C — Ledeburite adjoining Ni-martensite in fusion boundary region; D — Eutectic graphite, minute Ni-martensite in fusion boundary region; E — Iron carbide layer in HAZ; F — Martensitic layer in HAZ

ary, as shown in Fig. 3F.

In the martensite-fine pearlite layer at a distance from the fusion line, martensite and fine pearlite exist in abundance, which indicates the mixing of martensite and fine pearlite.

The fine-laminated pearlite layer which approaches the base metal has a matrix laminated with fine pearlite.

At the finely laminated pearlite layer the pearlite in the base metal becomes very finely laminated pearlite.

Ni-Fe Filler Metal. Figure 4 shows solidified microstructures of the fusion boundary area deposited with 50%Ni-50%Fe filler metal.

1. Deposit metal — In this region, a Ni-Fe-C alloy is produced and tiny spheroidal graphite is crystallized, as shown in Fig. 4A. The graphite is particularly numerous in the vicinity of the fusion boundary.

2. Fusion boundary region — In the center of the bead, Ni-Fe martensite adjoins ledeburite eutectic, as shown in Fig. 4B. From the circumference to the edges of the bead, Ni-Fe martensite and ledeburite eutectic continue towards a finely laminated pearlite matrix, as shown in Fig. 4C. At the center, Ni-Fe adjoins ledeburite eutectic and at the circumference, Ni-Fe martensite adjoins ledeburite eutectic. The ledeburite eutectic grows to the Ni-Fe side and connects with Ni-Fe martensite. This martensite is a large leaf-like one. Ni-Fe martensite is present and mixes with the large leaf-like martensite and minute martensite, and eutectic graphite precipitates, as shown in Fig. 4D. As shown in Fig. 4E, a great amount of eutectic graphite and minute martensite precipitates in a jumble, and these adjoin the laminated pearlite matrix.

3. HAZ — In the center and at the edges of the bead, an iron carbide layer appears, as shown in Fig. 4F. In the circumference, the layer is not apparent.

A fine-laminated pearlite layer is adjacent to the carbide layer and where the ledeburite eutectic disappears.

The finely laminated pearlite layer has the structure its name implies.

Commercial CIA-2 (AWS ENiFe-CI) Welding Rod. Figure 5 shows solidified microstructures in the fusion boundary area influenced by CIA-2(Ni55-Fe45 carbon-coated filler metal) welding rod. The structure of the fusion boundary is shown in Fig. 5A.

1. Deposit metal — As can be seen in Fig. 5B, network eutectic-graphite is precipitated into the Ni-Fe deposit region which contains a small amount of graphite nodule. This network graphite is thought to be net-shaped graphite coming from decomposed Ni_3C.

2. Fusion boundary region — In the center of the bead, Ni-Fe adjoins the iron carbide layer, and approaching the edges as shown in Fig. 5C, Ni-martensite precipitates and eutectic graphite adjoins the finely laminated pearlite matrix of the cast iron base metal.

3. HAZ — The portion partially melted by the heat from the filler metal appears as ledeburitic structure during solidification and the nonfused portion becomes fine-laminated pearlite.

The iron carbide layer at the center and the edges of the bead contain ledeburite.

The finely laminated pearlite layer is very thick, having been measured to be around 1.4 mm (0.06 in.) in the center and around 3.2 mm (0.13 in.) at the edges.

Fe Filler Metal. Figure 6 shows solidified microstructures in the fusion boundary area of the deposited Fe filler metal. The structure of the deposit metal is pearlite and that of the fusion boundary is white iron, as shown in Fig. 6A.

1. Deposit metal — Fe-C-5i alloy is constituently formed in this region, having a pearlite matrix.

2. Fusion boundary region — The boundary between pearlite in the Fe side and the ledeburitic eutectic is the fusion line, as can be seen in Fig. 6B. As shown in Fig. 6C, deposit metal in the vicinity of the fusion line has a columnar crystal structure of ferrite and pearlite.

3. HAZ — A relatively thick iron carbide layer appears along the fusion line, as shown in Fig. 6D.

A eutectic graphite crystallized layer was not observed in the center of the bead, but appeared at the circumference and the edges of the areas that underwent a relatively slow cooling rate, as can be seen in Fig. 6E. The thickness of this layer is about 0.21 mm (0.01 in.), and it has a pearlitic matrix.

The base metal adjoining the carbide layer or eutectic graphite-crystallized layer is very finely laminated pearlite.

The laminated pearlite layer of the base metal becomes finely laminated.

Thickness of Iron Carbide Layer

Average values of thickness of the iron carbide layer in HAZ for various filler metals are indicated in Table 4. Thickness of the carbide layer varies and the layer

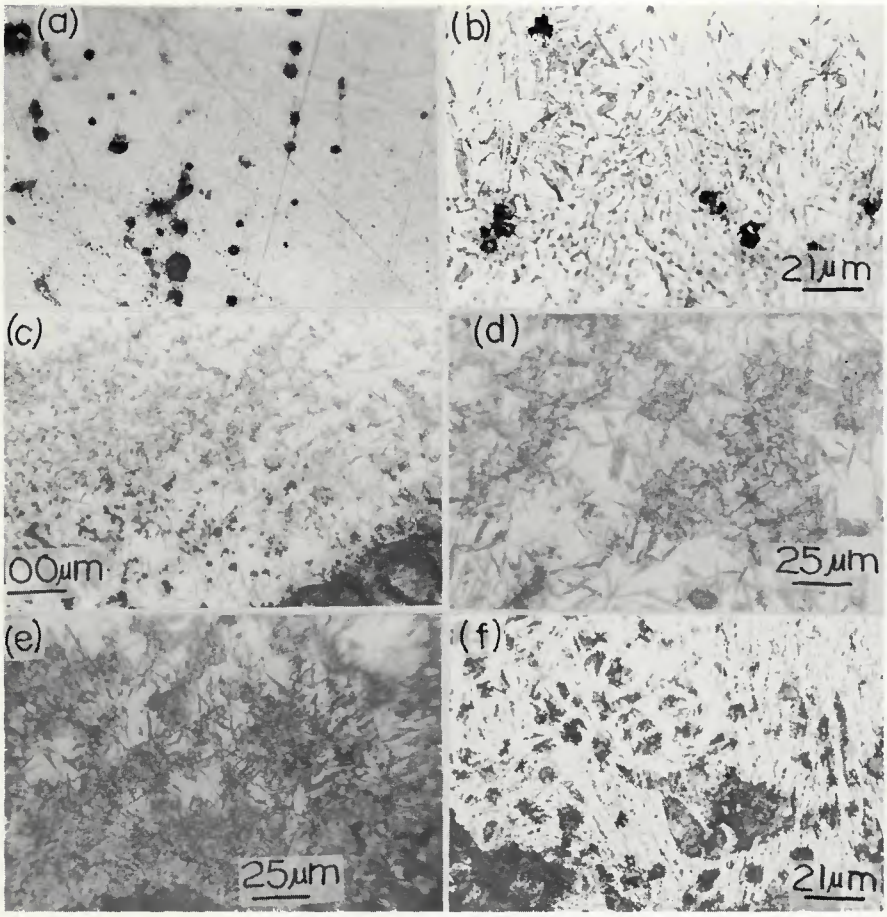

Fig. 4 — Microstructures of deposited metal fusion boundary area with Ni-Fe filler metal added by plasma arc (Nital etch). A — Tiny spheroidal graphite in Ni-Fe alloy of deposited metal; B — Ni-Fe martensite adjoining ledeburite in fusion boundary region; C — Ni-Fe martensite, eutectic graphite in fusion boundary region; D — Large leaf-like Ni-Fe martensite and eutectic graphite in fusion boundary region; E — Minute Ni-Fe martensite and eutectic graphite adjoining finely laminated pearlite matrix in fusion boundary region; (f) — Iron carbide layer in HAZ

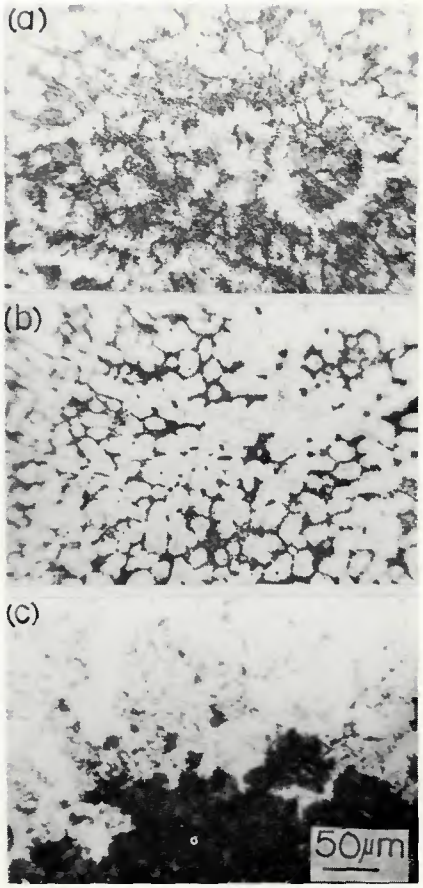

Fig. 5 — Microstructures of fusion boundary of FGI deposited with CIA-2 (AWS ENiFe-CI) welding rod by plasma arc (Nital etch). A — Deposited fusion boundary; B — Eutectic graphite precipitated within deposit metal; C — Ni martensite in contact with fine pearlite matrix

disappears in places. For the Ni system filler metal, the carbide layer is thicker in the center of the bead where the plasma flow hits it intensely and is thin at the edges. However, by using the Fe filler metal, the layer is thicker in the area from the circumference to the edges than it is in the center. Generally the carbide layer is thicker for Fe filler metal than for Ni system filler metal. This fact is thought to be due to the differences in the melting points of the filler metals. Ni and Fe have higher freezing points than cast iron. In such a case, the melting and solidification of base metal adjacent to deposit metal proceeds at a different rate from deposit metal, causing the fusion to form as a ledeburitic eutectic layer. Accordingly, since the melting point of Fe is higher than that of Ni and Ni-Fe, a large fusion of base metal cast iron occurs for Fe filler metal and the iron carbide layer appears subsequently thicker in the fused region.

Fusion Boundary Hardness

Figure 7 shows the results of microhardness tests across the deposit fusion boundary lines of Ni, Ni-Fe and Fe filler metals. The Vickers microhardness was measured with a loading of 500 g (17.6 oz), with care taken to avoid the graphite cavities. The hardness of Ni-martensite and Ni-Fe martensite was high, around VHN 675 and VHN 725, respectively. The hardness of the carbide layer was very high, around VHN 610 to 860 for Ni and Ni-Fe filler metals. However, it was slightly lower, around VHN 490 to 530, for Fe filler metal. The hardness was approximately VHN 550 in the martensitic area of HAZ, VHN 450 in martensitic-fine pearlite area and around VHN 400 to 450 in the fine laminated pearlite layer.

Electron Probe Microanalysis of the Fusion Boundary

Figures 8 and 9 show the results of EPMA traces across the deposit fusion boundary using Ni and Ni-Fe filler metals. A diffusing layer with a thickness of about 0.2 mm (0.008 in.) is recognized to exist across the fusion line. Ni content changes in the carbide layer produce a concentrated gradient. This indicates that Ni diffuses from the deposit metal to the HAZ.

Discussion

Without the Use of Filler Metal

The cast iron where the plasma arc directly strikes it is completely melted and the liquid becomes ledeburitic eutectic structure after solidification. In the center of the fusion region, the structure seems to be hypoeutectic white cast iron (Ref. 15), but the fine ledeburitic structure obtained in the vicinity of the fusion boundary is indistinguishable hypoeutectic from hypereutectic white cast iron. The formation of this ledeburite eutectic is due to a rapid cooling effect, since no composition change in the fusion region and no reaction with the plasma gas could have occurred in the short arc time. Furthermore, with a long arc time a higher heat input lowers the cooling rate, but as the rate is yet far higher than in castings, the major cause of the formation may be a relatively high cooling rate.

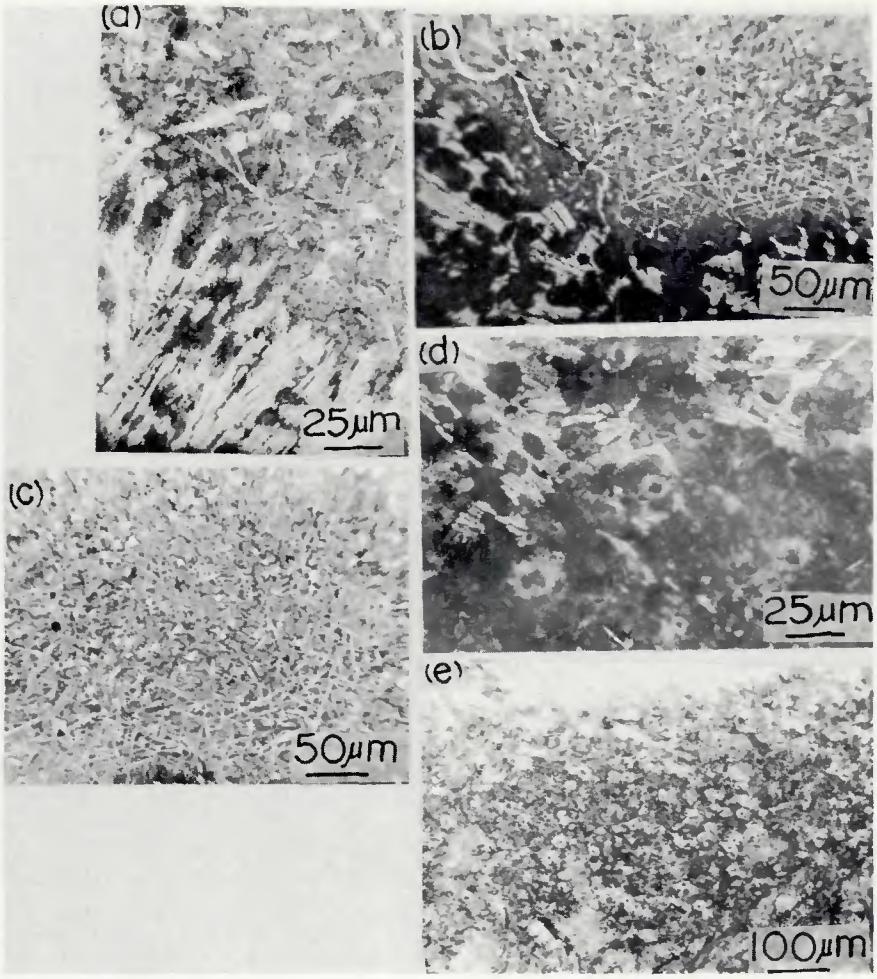

Fig. 6 — Microstructures of fusion boundary and HAZ of FGI deposited with Fe filler metal by plasma arc (Nital etch). A — Deposited fusion boundary region; B — Fusion boundary region having ledeburite adjacent to pearlite of Fe deposit metal side; C — Columnar structure consisting of ferrite and pearlite in fusion boundary of deposit metal; D — Iron carbide layer in the HAZ; E — Eutectic graphite layer appearing in the HAZ

Table 4—Averaged Thickness of Iron Carbide Layer in the HAZ Using Filler Metals

	Position of the layer in the bead (mm)	
Filler metal	Center	Edge
Ni	0.169	0.05
Ni-Fe	0.124	0.04
Fe	0.254	0.415

Especially in the vicinity of the fusion boundary, the molten iron freezes as white iron due to an undercooled phenomenon. As the arc time increases, so does the temperature in the completely molten region, which causes a reaction with the plasma shielding gas, and the loss of carbon and silicon to occur. In the fusion boundary region, the amount of crystallized graphite is less in the center of the bead than in the circumference. This fact is related to the cooling rate during solidification, but the formation of graphite nuclei is considered to be avoided by agitation in the center of the bead from the intense plasma gas flow.

Figure 10 shows a schematic illustration of the structure in the fusion boundary area of FGI locally melted by plasma arc. For a low heat input, the structure in the HAZ is martensite due to a high cooling rate. Minute martensite appears on the fusion line as a result of a supercooled effect. Martensite in the HAZ consists of coarse α-martensite adjacent to the fusion line and fine β-martensite precipitating ϵ-carbide in the base metal side. Martensite is known to be easily decomposed to under $M_s$point (Ref. 16). This β-martensite is thought to be formed by the composition of α-martensite. Accordingly, the martensite in the base metal side is thought to be subjected to a short-time tempering. For high heat input, the fusion region becomes white cast iron. However, very small flake graphite appears in a portion of the molten iron in the vicinity of the fusion line, which seems to be precipitated as a secondary graphite during solidification. This secondary graphite is crystallized from the liquid phase; namely, it is supercooled graphite. A relatively low cooling rate resulting from a high heat input has an effect on the graphitization in the vicinity of the fusion line and decreases the partial supersaturation of carbon into austenitic matrix in HAZ. The result is a HAZ with a finely laminated pearlite structure.

Solid solution phenomenon with a dissolution and diffusion of carbon from flake graphite into an austenitic matrix in the HAZ occurs in greater quantity as the fusion line is approached. A wide area in the HAZ contains carbon solid solution. The amount of solid solution in the HAZ is dependent upon time and temperature, and the structures such as martensite, fine pearlite and laminated pearlite depend upon the solid solution of carbon and the cooling rate. The migration of carbon has scarcely occurred before a very finely laminated pearlite structure borders the unaffected base metal. The carbon solid solution process is comprised of a dissolution reaction at the interface between graphite and matrix, and of a diffusion process in which the carbon atom diffuses into the matrix. The rate of carbon solid solution has been reported to be controlled by dissolution reaction (Ref. 17). It is pointed out from this result that the interface concentration between flake graphite and the matrix does not reach the saturation limit. This indicates that the melting point of the matrix around flake graphite is not lowered significantly. This is understood also from the fact that the matrix immediately adjacent to the flake graphite gives no evidence of having been fused and solidified as ledeburite eutectic.

With the Use of Filler Metal

Figure 11 illustrates schematically the structures of the fusion boundary area of FGI after depositing filler metal by plasma arc. In the fusion boundary region of deposit metal side, Ni-martensite (Figs. 3C, 4D), eutectic graphite (this is thought to be graphite which Ni_3C decomposes partially (Refs. 18, 19), minute Ni-martensite (Fig. 3D), and small flake graphite (Figs. 3D, 4D) are precipitated when Ni and Ni-Fe filler metal are used, and needle-like ferrite (Figs. 6B and C) is precipitated with the use of Fe filler metal, which is recognized as a supercooled effect in this region. The structure in the HAZ varies with the differences in the melting points

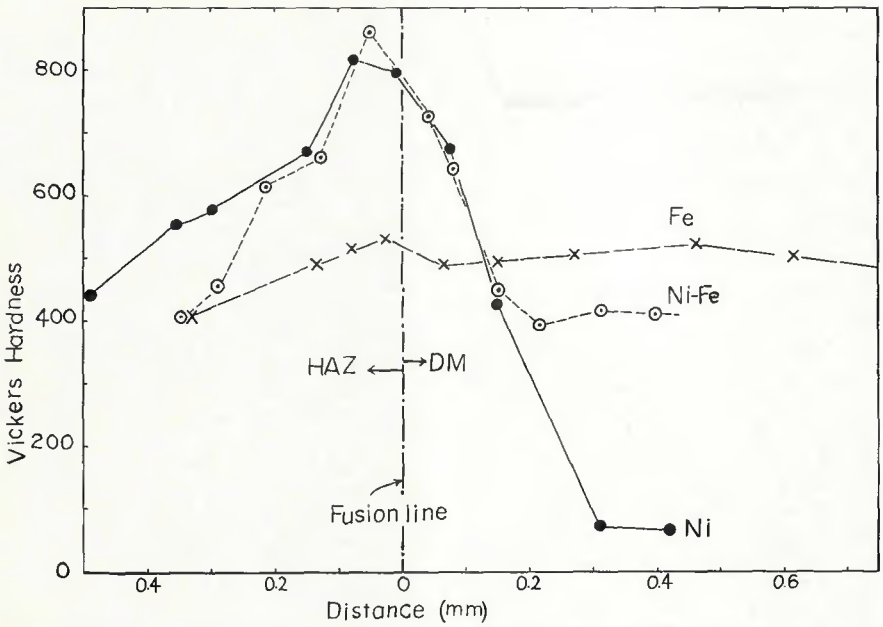

Fig. 7 — Hardness of FGI across fusion boundary using Ni, Ni-Fe and Fe filler metals

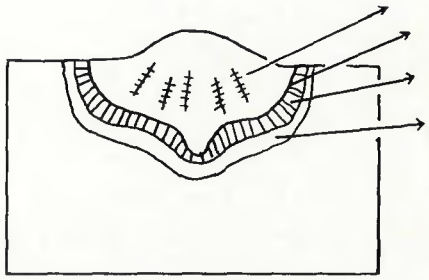

Fig. 10 — Schematic illustration showing the structures of each region of FGI locally melted by plasma arc without the addition of filler metal

of filler metals. Using Ni filler metal (Fig. 11A), which has a melting point nearest to cast iron, the HAZ is composed of a relatively thin iron carbide layer, martensitic layer, martensitic-fine pearlite mixed layer and laminated pearlite layer. Using Ni-Fe filler metal, as shown in Fig. 11B, the HAZ consists of an iron carbide layer and a laminated pearlite layer. With the use of Fe filler metal, which has the highest melting point, a relatively large fused region in the base metal is produced and the HAZ contains a relatively thick iron carbide layer, a eutectic graphite-crystallized layer and a laminated pearlite layer — Fig. 11C.

The hardness at the Ni-martensite and iron carbide layers in the fusion boundary area was very high where the molten metal existed. However, with the use of Fe filler metal, the hardness was slightly lower in the ledeburitic eutectic area where a diffusion of Fe from deposit metal occurred. Using Fe filler metal, the hardness changes little in the fusion boundary.

In filler metal with a low melting point, the heat migration from deposit metal into the base metal and the fused region of the base metal is limited. Therefore, the carbide layer becomes thin and a martensitic layer in the HAZ is produced by a rapid cooling. In filler metal with a high melting point, the heat migration from the deposit metal is considerable and the carbide layer in the HAZ become thick. In this instance, a rapidly cooled structure such as martensite does not appear, but instead a layer of crystallizing eutectic graphite is formed. Generally, when using filler metal, a white iron layer with massive carbide is formed on the base metal side in the fusion boundary region. This carbide layer is considered to appear as a result of the fusion of base metal which proceeds during solidification of deposit metal. Thus, the formation of white iron is unsuitable for a good weldment. The structure of the HAZ can be controlled by the magnitude of heat input from the arc and the kind of filler metal. The use of the filler metal having a melting point near the base metal in conjunction with a high heat input makes the white iron layer thin or disappear, and the rapidly cooled martensite formation and the partial supersaturation of carbon in the HAZ is avoided. Namely, by using carbon-coated Ni filler metal CIA-1 (AWS ENi-CI) and a high heat input, the cooling rate in the fusion boundary area should be as low as possible so as to prevent white iron structure formation and to provide graphitized structure, as noted below. Deposit metal has a Ni austenitic matrix with many slim graphites, as shown in Fig. 12A. In the fusion boundary region at the center of the bead, Ni-

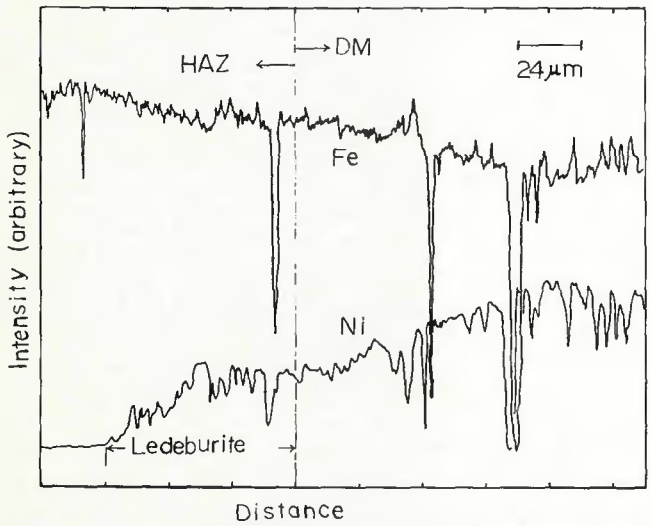

Fig. 8 — EPMA traces of Ni-K_α and Fe-K_α rays across fusion boundary of FGI deposited with Ni filler metal by plasma arc

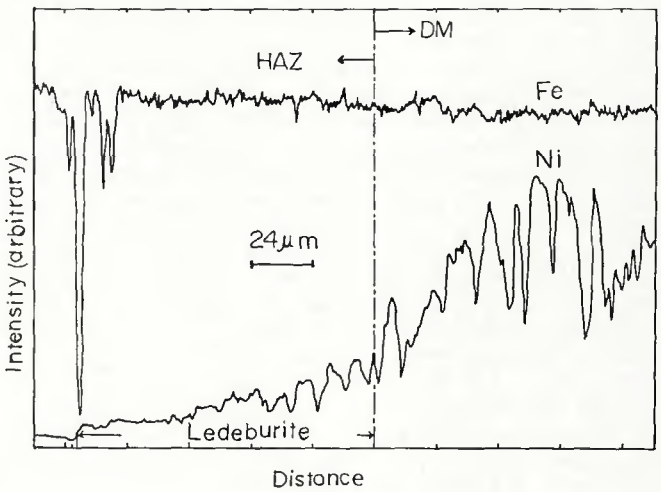

Fig. 9 — EPMA traces of Ni-K_α and Fe-K_α rays across fusion boundary of FGI deposited Ni-Fe filler metal by plasma arc

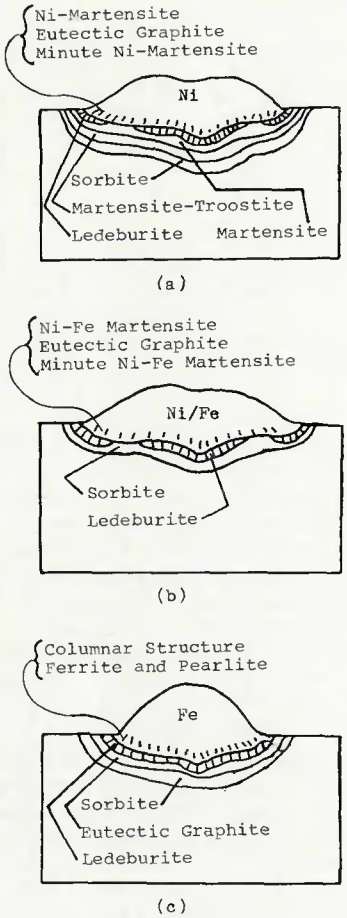

Fig. 11—Schematic illustrations showing the structures of fusion boundary area of FGI with filler metal deposited by plasma arc. A—Deposited with Ni filler metal; B—Deposited with Ni-Fe filler metal; C—Deposited with Fe filler metal

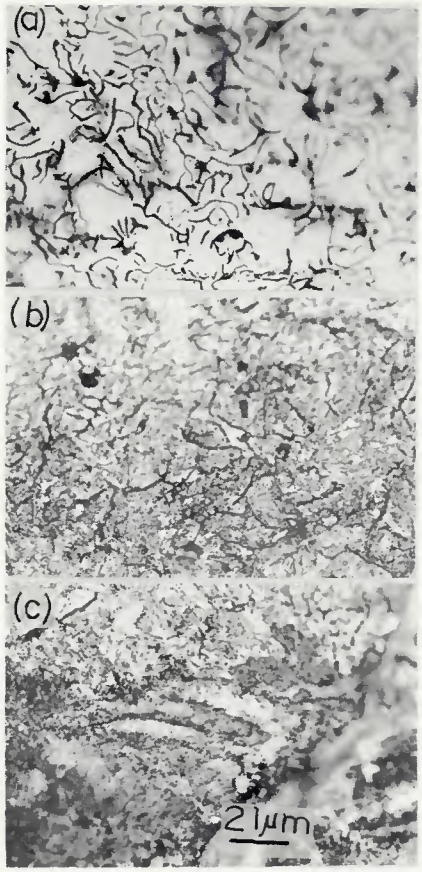

Fig. 12—Microstructures of fusion boundary area of FGI deposited with CIA-1 (AWS ENi-CI) welding rod by plasma arc (Nital etch). A—Many slim graphites within Ni austenitic matrix in deposit metal; B—Ni-martensite and slim graphite in fusion boundary region; C—Fine-laminated pearlite matrix adjacent to Ni-martensite

martensite (Fig. 12B) precipitates slim graphite to the Ni metal side which adjoins the laminated pearlite matrix (Fig. 12C) with flake graphite in the HAZ. In the area from the circumference to the edges, Ni-martensite with slim graphite in the Ni metal side adjoins a laminated pearlite matrix which has slender flake graphite and precipitated eutectic graphite resulting from a small portion of fused base metal. In the center of the bead, the HAZ is laminated pearlite with flake graphite, but at the edges of the bead, the HAZ includes a eutectic graphite-crystallized layer with slender flake graphite and laminated pearlite layer. In this case, the HAZ is comprised of a eutectic graphite-precipitated layer and a relatively thick pearlite layer, which is a structure that tends to graphitize.

Finally, the diffusion of Ni element in the filler metal into the HAZ will be discussed. It may be important to consider whether solute in the filler metal can actually diffuse into the HAZ or not. In the welding of cast iron, the liquid portion of the HAZ is solidified as white iron. Therefore, the chemical composition of the liquid is altered by means of the diffusion of elements from the deposit metal into the HAZ. The desire is to avoid white iron formation. Figures 8 and 9 show that Ni diffuses into the carbide layer in the HAZ. With the depositing of filler metal, partial melting of the base metal in the vicinity of deposit metal occurs due to the heat from the deposit metal side, and this interaction between the deposit metal and the partially fused metal may play an important role in the diffusion of Ni into the HAZ. Accordingly, the diffusion of Ni from the deposit metal into the HAZ occurs at least until the base metal is fused.

Conclusions

Microstructural changes in the fusion region, deposited filler metal, fusion boundary region and HAZ of flake graphite cast iron locally melted by plasma arc with and without filler metal were investigated. The principal results and conclusions are as follows:

1. Without the use of filler metal, the structure in the fusion region is that of a hypoeutectic white cast iron in the center and that of fine ledeburite eutectic in the vicinity of the fusion line.
2. In the fusion boundary region where a supercooled phenomenon can occur, minute martensite precipitates along the fusion line with low heat input and secondary graphite precipitates with high heat input.
3. The HAZ is composed of white martensite, dark martensite and martensite-fine pearlite layers with low heat input, and of laminated pearlite and laminated pearlite-ferrite layers with high heat input.
4. Solid solution of carbon from flake graphite in the matrix occurs mostly in the HAZ and no evidence of fusion due to a partial lowering of the melting point of the matrix adjacent to flake graphite can be found.
5. With the use of filler metal, the structure of deposit metal is that of a Ni austenitic matrix precipitating tiny graphite nodule or slim graphite for Ni and Ni-Fe filler metals and a pearlitic matrix for Fe filler metal.
6. In the fusion boundary region, Ni-martensite, eutectic or slim graphite, and minute Ni-martensite precipitate with Ni system filler metals and a columnar structure of ferrite and pearlite exists for Fe filler metal.
7. The HAZ is composed of iron carbide, martensite, martensite-fine pearlite and laminated pearlite for Ni filler metal; of iron carbide and laminated pearlite for Ni-Fe filler metal; and of iron carbide, eutectic graphite and laminated pearlite for Fe filler metal. The structure of HAZ is considered to vary with the melting point of the filler metal.
8. Iron carbide layer in HAZ is thicker for Fe filler metal than for Ni or Ni-Fe filler metal because of the difference of freezing points of the filler metals.
9. Hardness in the Ni-martensite and iron carbide layers of the fusion boundary region is very high. However, it is slightly lower in the carbide area when Fe filler metal is used.
10. The formation of carbide and martensitic layers can be avoided by a relatively longer arc time, that is, higher heat input, and by the use of filler metal having a melting point close to base metal.
11. It is obvious from the presence of Ni concentration gradient in the iron carbide layer that the diffusion of Ni from the deposit metal to the HAZ can occur at least until the base metal is fused.

Acknowledgments

The author would like to thank Mr. H. Yamaguchi (Hitachi Ltd.) for his help and advice in the plasma arc experiment; Mr. S. Yamada, Mr. K. Enami and K. Wako for

the preparation of the specimens and the filler metals; Mr. S. Oki for the EPMA work; and Mr. S. Takeyama for the element analysis.

References

1. Young-Won, K., Strutt, R. R., and Nowotny, H. 1979. Laser melting and heat treatment of M2 tool steel: a microstructural characterization. *Metallurgical Trans.* 10A:881-886.

2. Strutt, R. R. 1981. Formation of rapidly melted surface layers by electron beam scanning. *Materials Science and Engineering* 49:87-91.

3. Hiller, W. 1976. Schweissen und thermisches behandeln von gusswerkstoffen mit dem electronstrahl. *Giesserei* 63:316-321.

4. Tomsic, M.J., and Jackson, C.E. 1974. Energy distribution in keyhole mode plasma arc weld. *Welding Journal* 53(3):109-s to 115-s.

5. Townshend, B., and Porter, E.O. 1959. Process welding of nodular and gray iron castings. *Welding Journal* 38(8):329-s to 334-s.

6. Homma, M., Wada, T., and Yamaya, K. 1960. Welding of cast iron and nodular graphite cast steel. *Sci. Rep.* 12:437-447.

7. Devletian, J.H. 1978. Weldability of gray iron using fluxless gray iron electrodes for SMAW. *Welding Journal* 57(7):183-s to 188-s.

8. Devletian, J.H. 1980. Aluminum's graphitizing effect in gray iron welds. *Welding Journal* 59(12):349-s to 354-s.

9. Homma, M., and Ishida, T. 1965. Changes in the graphite structures of flake graphite and spheroidal graphite cast irons by the fusion in a short time. *Sci. Rep.* RITU, A 17(1):1-12.

10. Eck, B.J., editor. 1978. Metals Handbook, Ninth Edition, Volume I. Properties and Selection: Irons and Steels. American Society for Metals.

11. Thielsch, H. 1952. Stainless steel weld deposits on mild and alloy steel. *Welding Journal* 31(1):37-s to 64-s.

12. Zitzelsberger, W. 1959. Das schweissen von ferrtishch geglühtem gusseisen mit kugelgraphit. *Schweissen und Schneiden* 11:416-427.

13. Ruge, J., and Zitzelsberger, W. 1958. Wolfram-Innertschweissen von gusseisen mit kugelgraphit. *Schweissen und Schneiden* 10(3):86-90.

14. Kase, T. 1925. On the equilibrium diagram of the iron-carbon-nickel system. *Sci. Rep.* RITU 14:173-218.

15. Okamoto, M., and Yoda, R. 1961. Atlas of Microstructures – Cast Iron. Yōkendō.

16. Okamoto, M. 1960. Iron and steel as an engineering material. Korona Limited, p. 136.

17. Ikawa, H., Shin, S., Nakao, Y., and Nishimoto, K. 1975. Dissolution phenomenon of graphite in spheroidal graphite cast steel during weld thermal cycles. *Journal of the Japan Welding Society* 44(3):229-235.

18. Wasserman, R.D., Quaas, J.F., and Broderick, J.P. 1957. Aspects of crack sensitivity in machinable deposits on cast iron. *Welding Journal* 36(5):481-488.

19. Sohn, J., Boam, W., and Fisk, H. 1953. Arc welding of ferritic and austenitic nodular cast iron. *Welding Journal* 32(10):823-833.